

Cannabinoids Disrupt Memory Encoding by Functionally Isolating Hippocampal CA1 from CA3

Roman A. Sandler ^{*1}, Dustin Fetterhoff ², Robert E. Hampson ², Sam A.
Deadwyler ² & Vasilis Z. Marmarelis¹

¹Department of Biomedical Engineering, University of Southern
California, Los Angeles, CA, USA

²Department of Physiology & Pharmacology, Wake Forest University,
Winston-Salem, NC, USA

June 16, 2017

Abstract

Much of the research on cannabinoids (CBs) has focused on their effects at the molecular and synaptic level. However, the effects of CBs on the dynamics of neural circuits remains poorly understood. This study aims to disentangle the effects of CBs on the functional dynamics of the hippocampal Schaffer collateral synapse by using data-driven nonparametric modeling. Multi-unit activity was recorded from rats doing an working memory task in control sessions and under the influence of exogenously administered tetrahydrocannabinol (THC), the primary CB found in marijuana. It was found that THC left firing rate unaltered and only slightly reduced theta oscillations. Multivariate autoregressive models, estimated from spontaneous spiking activity, were then used to describe the dynamical transformation from CA3 to CA1. They revealed that THC served to functionally isolate CA1 from CA3 by reducing feedforward excitation and theta information flow. The functional isolation was compensated by increased feedback excitation within CA1, thus leading to unaltered firing rates. Finally, both of these effects were shown to be correlated with memory impairments in the working memory task. By elucidating the circuit mechanisms of CBs, these results help close the gap in knowledge between the cellular and behavioral effects of CBs.

Author Summary

Research into cannabinoids (CBs) over the last several decades has found that they induce a large variety of oftentimes opposing effects on various neuronal receptors and processes. Due to this plethora of effects, disentangling how CBs influence neuronal circuits has proven challenging. This paper contributes to our understanding of the circuit level effects of CBs by using data driven modeling to examine how THC affects the input-output relationship in the Schaffer collateral synapse in the hippocampus. It was found that THC functionally isolated CA1 from CA3 by reducing feedforward excitation and theta information flow while simultaneously increasing feedback excitation within CA1. By elucidating the circuit mechanisms of CBs, these results help close the gap in knowledge between the cellular and behavioral effects of CBs.

*Corresponding Author: rsandler00@gmail.com

1 Introduction

Recent years have seen a resurgence of interest in the therapeutic role of cannabinoids (CBs) for several diseases and neuropsychiatric disorders such as psychosis, anxiety disorders, PTSD, and multiple sclerosis [1, 2]. In particular, CB agonists have shown promising but mixed results in the treatment of epilepsy, as various types of agonists at various doses have been shown to be both pro- and anticonvulsant [3, 4, 5, 6, 7, 8, 7]. Parallel to increasing therapeutic research, much work has been done on the chemical structure of various cannabinoids and cannabinoid receptors, along with their cellular interactions and pharmacology [9].

Nonetheless, between the large bodies of literature on cannabinoids from chemical, disease, and behavioral perspectives, much less work has been done to explore the effects of cannabinoids on the neural circuit level. This is particularly important since a wide range of complex and often opposing effects have been attributed to cannabinoids on a molecular and cellular level. For example, cannabinoid activation of CB1 receptors, which are found on both pyramidal cells and interneurons, reduces the quantity of neurotransmitter released during an action potential; consequently, increased extracellular cannabinoid levels reduce both excitatory (glutamatergic) and inhibitory (GABAergic) transmission [10]. Furthermore, cannabinoids have been shown to interact with astrocytes [11], mitochondria [12], glycine receptors [13], vanilloid receptors [14], potassium ion channels [15], and to reduce GABA and glutamate reuptake [16, 17]. Consequently, it is very difficult to extrapolate the emergent network level changes simply from a catalogue of effects cannabinoids have at a cellular/molecular level.

Here, we studied the effects of Δ^9 -tetrahydrocannabinol (THC) on hippocampal networks during memory encoding using spiking activity recorded in rodents in-vivo performing the Delayed-NonMatch-to-Sample (DNMS) working memory task. Multivariate autoregressive (MVAR) models were used in both control and THC sessions to estimate feedforward and feedback dynamical filters, which are akin to the waveform shapes of the CA3→CA1 EPSP and CA1 afterhyperpolarization, respectively [18]. MVAR models, which are a type of linear nonparametric model, are 'data-driven' in the sense that they estimate model parameters directly from recorded neural spiketrains and, unlike more biologically realistic models, make very few *a priori* assumptions on the nature of the neural dynamics [19, 20]. This characteristic makes them particularly well suited for this study, since as previously mentioned the emergent effects of THC on neural circuits are highly complex and unclear. Overall our results suggest that cannabinoids impair memory encoding by functionally isolating CA1 from CA3 via reduced theta information flow and altered excitatory-inhibitory balance across the Schaffer collateral synapse.

2 Results

2.1 Changes in rate and temporal coding under Cannabinoids

To evaluate the effects of exogenous cannabinoids on the hippocampal network 1 mg/kg THC was injected intraperitoneally into $N = 6$ rodents during certain sessions while they were performing a DNMS task (Fig. S1). All data was previously used in a study on the effects of cannabinoids on hippocampal multifractality [21, 22]. Briefly, in the sample phase, the rats were presented one of two levers. After a variable length delay, both levers were presented in the match phase and the rat had to choose the opposite lever to receive a reward. On the behavioral level, it was found that THC reduced rodent-performance on the DNMS task by about $12.2 \pm .6\%$ (Fig. 1a, [23]). This corresponds to a 24.4% impairment relative to baseline performance at 50%.

While performing the DNMS task, single-unit activity was recorded from the hippocampal CA3 and CA1 regions using a multi-electrode array. There were no significant mean firing rate (MFR) differences between THC sessions and control sessions in either CA3 or CA1 cells ($P = .502$, Fig. 1b). No MFR differences were seen whether considering the entire session or only times around the DNMS sample phase, or whether considering all cells or only sample-presentation cells (see below). The lack of any cannabinoid-induced changes in firing rates at this dosage has been observed in previous studies [24, 25].

Two types of temporal coding were identified in the recorded spiketrains. First, on slower timescales, several neurons fired preferentially in response to lever presentation in the sample phase of the DNMS task [26]. It was found that THC reduced the proportion of sample-presentation cells in both CA3 and CA1 by roughly equal amounts ($\Delta = 13 \pm 4\%$, $P < .001$; Fig. 1c). Interestingly, some sample-presentation cells lost all of their preferential firing in THC sessions (Fig. 1d); this contrasts with place cells whose receptive field stays largely intact under cannabinoids [27]. There was an insignificant trend connecting sample-presentation cell reduction with behavioral deficits ($R^2 = .27$, $P = .052$, Fig. S3a).

On faster timescales, it was found that several CA3 and CA1 neurons had theta band rhythmicity (4-7 Hz). Hippocampal theta oscillations are known to be intimately related to cognitive function [28, 29, 30] and have previously been linked to performance in the DNMS task [31]; furthermore, theta oscillations are known to be reduced by systemic injections of cannabinoids on both the single unit [24] and network level [32]. It was found that CA1 theta power was slightly but significantly reduced in THC sessions ($\Delta = 2.52\%$, $CI : [.61, 4.4]\%$, $P = .004$; Fig. 1e). A similar, albeit slightly weaker, theta power reduction was seen in CA3 cells ($\Delta = 1.94\%$, $P = .045$; Fig. S2). Interestingly, in both cases, the significant reduction of theta power occurred at 5-6Hz, which is lower than the observed theta peak. Unlike previous results in a different task [24], the reduction in CA1 theta power was not found to be correlated with behavioral deficits in the DNMS task ($P = .674$, Fig. S3b).

Overall, these results show that THC has minor effects on the actual neuronal spiketimes: quantity of spikes (MFR) was not affected and spike rhythmicity

(theta oscillations) were only slightly affected. Furthermore behavioral deficits induced by cannabinoids could not be explained by any of these factors, which are the traditional markers of rate and temporal coding in the hippocampus.

2.2 Systems Analysis

The remainder of the study will focus on systems analysis of the Schaffer collateral synapse connecting CA3 to CA1, and how this synapse is affected by THC. Systems analysis aims to identify the input-output "blackbox" by which the input spiketrains are transformed into the output spiketrain. On a more abstract level, it aims to identify how the information encoded in CA3 is propagated into CA1. This is distinct from the *signal* analysis done in the previous section which only looks at features of individual spiketrains rather than the causal relationship between multiple spiketrains as done in systems analysis.

The relationship between an arbitrary number of input CA3 spiketrains and the output CA1 spiketrain was modeled using a multivariate autoregressive model described by Eq. 1 and an example of which is pictured in Fig. 2a. Each system consists of N input CA3 neurons and N feedforward filters describing the dynamical input-output relationship between the given CA3 and CA1 neurons (Fig. 2b). Intuitively, these filters can be thought of as the EPSP elicited in the output CA1 neuron in response to an action potential (AP) in the input CA3 neuron. However, unlike EPSPs which traditionally only encapsulate ion-conductances from neurotransmitter-gated ion channels, the "black-box" nature of the feedforward filters means they also include more complex dynamical effects such as dendritic integration, spike generation, active membrane conductances, and feedforward interneuronal inhibition (thereby allowing the filters between two pyramidal cells to be inhibitory). Each model also includes a feedback (autoregressive) filter which describes the effects of past output spikes onto the output present. This filter, which can be intuitively thought of as the afterhyperpotential (AHP) [33] includes intracellular processes such as the absolute and relative refractory periods, slow potassium conductances, and I_h conductances. It also includes more complex intercellular processes such as the recurrent connections between CA1 pyramidal cells and interneurons [34]. Neuronal connectivity was estimated using a stepwise input selection procedure. Filter parameters were estimated with Laguerre basis regression using neuronal activity around the sample phase. Model significance was verified using ROC plots and shuffling methods (see supplementary methods).

A representative connectivity grid from a recorded THC session with 10 recorded neurons (4 CA3, 6 CA1) is shown in Fig. 2a. Fig. 2b shows a sample system from this session between 3 CA3 pyramidal cells and 1 CA1 pyramidal cell. Note that two of the feedforward filters are excitatory (above the x-axis) while the third has both excitatory and inhibitory components, presumably arising through feedforward inhibition involving interneurons [35, 36]. The system also involves a feedback filter which shows a relatively long refractory period (~ 40 ms) followed oscillatory bursting activity. Oscillations in the CA1 pyramidal cell AHP are a well known phenomena caused by slow K^+ and I_h conduc-

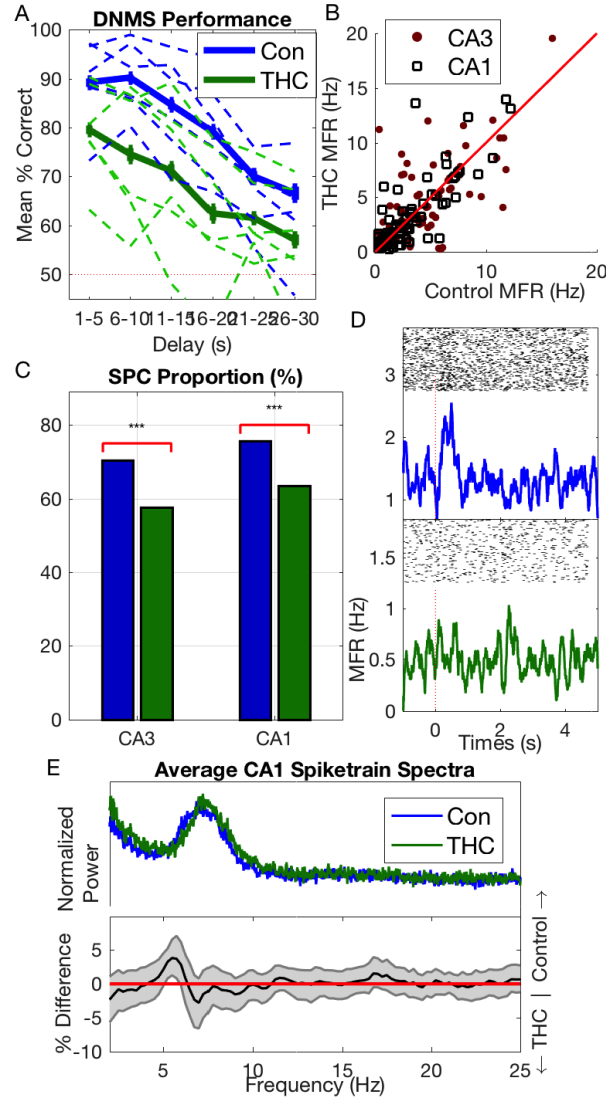


Figure 1: (A) Behavioral performance on Delayed-NonMatch-to-Sample (DNMS) task in both control and THC sessions. Dashed lines show individual animal performance, while solid lines show mean performance over all animals. Bars indicate SEM. Dashed red line indicates performance at chance level. (B) Individual neuron mean firing rate (MFR). (C) Sample-presentation cell proportion in CA3 and CA1 cells in control & THC sessions ($***=P < .001$). (D) Example of a sample-presentation cell in a control session (top) which lost its firing specificity under THC (bottom). X-axis shows MFR (Hz) (E) Average CA1 spiketrain spectra (top). Bottom shows mean difference in individual cell spectra (thus it is not simply the difference between the signals in above which are averaged over whole population). Gray error bounds indicate 99% confidence bounds. In (B) and (E), only neurons recorded in at least one control & THC session were included. Results for neurons recorded in several control or THC sessions were averaged over those sessions.

171 tances, and these oscillations are known to lead to theta resonances [37, 38, 18].
 172 In order to study the filter oscillations more closely, the filter frequency spec-

173 tra were plotted in Fig. 2c. Both feedforward excitatory filters were found to
 174 have peaks in the high theta range (8-9 Hz). Intuitively, this can be understood
 175 to mean that information encoded in the theta range in these input neurons is
 176 preferentially transmitted to the output CA1 neuron. Furthermore, the feedback
 177 filter has a low theta resonance of 3.5 Hz. Significance metrics for the displayed
 178 system is shown in Fig. S4, and additional systems are shown in Fig. S5. All
 179 together 66% (707/1068) of all systems were found to be significant and 2139
 180 feedforward and 707 feedback filters were obtained. THC was found to reduce
 181 the number of significant models per session ($\Delta = -7.4\%$, $P = .011$), but the
 182 predictive power of significant models, as measured by AUC (see supplementary
 183 methods), was unaltered ($P = .24$).

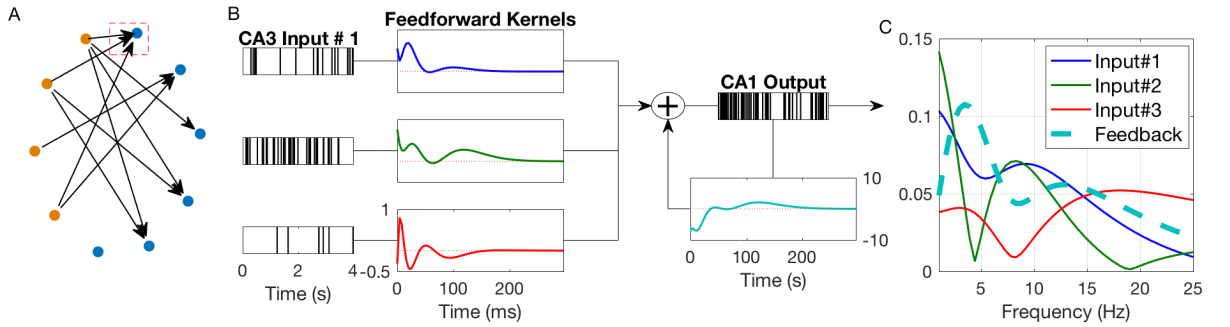


Figure 2: (A) Example connectivity grid of 4 CA3 neurons (orange) and 6 CA1 neurons (blue) recorded during a single session. Note that 1 CA1 neuron has no significant granger-causal inputs. Each line represents a causal connection between those neurons, as encapsulated by a feedforward filter. (B) Example system of CA1 neuron enclosed by the red box in (A). Diagram shows 3 input CA3 spiketrains followed by their respective feedforward filters which are summed with the feedback filter to generate the output CA1 spiketrain. All feedforward filter are plotted with the same y-axis scale. Dashed red line in filter boxes indicates x-axis. (C) Normalized filter spectra computed of feedforward and feedback filters from (B).

184 To study how THC affects system dynamics on a population level, we ex-
 185 amined how features change in the entire sample of control and THC filters.
 186 The average filter frequency profile for both control and THC sessions is shown
 187 in Fig. 3a,b (top). Both feedforward and feedback spectra are found to have
 188 clear theta band peaks, thus generalizing the trend seen in the example system
 189 of Fig. 2. This is consistent previous reports which show that CA3 propagates
 190 strong theta rhythms to CA1 [39, 40] and also that CA1 is capable to gener-
 191 ating endogenous theta rhythms [41]. THC produced a significant decline in
 192 the theta power of the feedback filters ($\Delta = 20.8\%$, $P < .001$; Fig. 3b). Note
 193 that the feedback filter theta reduction is about 10x stronger than the theta
 194 reduction found in the CA1 spiketrain signals (Fig. 1e). No reduction in theta
 195 power was found in the feedforward filters ($P = .61$, Fig. 3a). This result sug-
 196 gests that cannabinoid-induced theta desynchronization results primarily from
 197 altered feedback properties rather than changes in CA3→CA1 dynamics.

198 Cannabinoids have been reported to affect network excitation-inhibition bal-

199 ance (EIB) [10, 42]. Particularly, there is much debate whether cannabinoids are
 200 pro- or anticonvulsants [8, 43, 44, 4, 6]. In order to examine the effects cannabi-
 201 noids have on network EIB, we quantified the excitation of the estimated filters
 202 using a metric called the excitatory index (EI), which is the ratio between pos-
 203 itive filter area and total filter area. It was found that THC had no significant
 204 effect on feedforward EI ($P = .14$); however, there was an insignificant trend
 205 showing that THC-induced decreases in feedforward EI were correlated with be-
 206 havioral deficits ($R^2 = .27, P = .063$, Fig. 3c). Additionally, THC reduced the
 207 number of casually connected CA3-CA1 neuronal pairs ($\Delta = -8.9\%$, $P < .001$).
 208 These findings, together with the THC-induced decrease of CA3→CA1 signifi-
 209 cant models, suggest that THC reduces the causal influence CA3 neurons have
 210 on CA1 spiketimes. In other words, THC can be said to functionally isolate
 211 CA1 from CA3. It was also found that THC significantly increased feedback EI
 212 ($\Delta = 3.5\%$, $P = .022$) and that the increased feedback EI was correlated with
 213 behavioral deficits ($R^2 = .38, P = .007$, Fig. 3d).

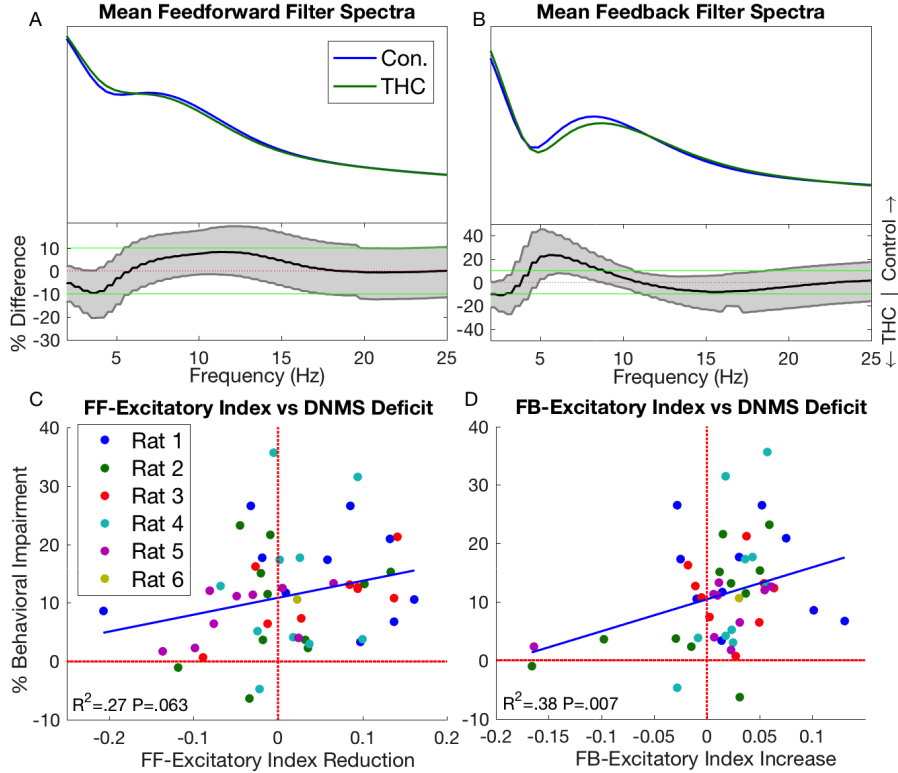


Figure 3: Average feedforward (A) and feedback (B) filter spectra in control and THC sessions (top), and their differences (bottom). Same format and analysis as Fig. 1a. (C) Correlation between feedforward filter excitatory index (EI) reduction and behavioral deficits. Each point represents a specific THC session, with points of the same color coming from the same animal. X-axis shows reduction in feedforward EI, while y-axis shows reduction in behavioral performance. Both reductions were taken relative to control sessions (see supplemental methods). (D) Same as (C) but for feedback EI increase.

2.3 PDM Analysis

The large quantity (>2800) and variability of the obtained filters describing the CA3→CA1 dynamic transformation presents a challenge of interpretation. Namely, how could one identify features from the entire filter population which are representative of the CA3→CA1 transformation rather than just the input-output relationship found in this or that particular pair of neurons. In essence this is an unsupervised learning problem which aims to identify hidden structure within the filter population for the purpose of knowledge discovery. Our group has developed the concept of the global principal dynamic modes (gPDMs) towards this effort [19, 45, 46]. The gPDMs are a system-specific and efficient basis set which contain the essential dynamic components of the filter population and are meant to be amenable to biological interpretation. One set of gPDMs were estimated from all (control and THC) obtained filters with the hypothesis that THC would primarily change the expression strength of the gPDMs rather than their specific shapes.

Fig. 4a,b shows the obtained feedforward and feedback gPDMs in both the time and frequency domain. Once again, the feedforward and feedback gPDMs represent the dominant independent components of feedforward and feedback kernels, respectively. The first feedforward gPDM was found to have almost all its energy in the 1st time bin, with an immediate decline thereafter. This gPDM represents near concurrent firing between CA3 and CA1 neurons and presumably results from both direct CA3→CA1 connections via the Schaffer collateral synapse [47, 48] and common inputs from the entorhinal cortex [49, 50]. The third feedforward gPDM, which is characterized by an initial inhibitory phase, presumably represents feedforward interneuronal inhibition which is prevalent in the CA3→CA1 connection [35, 36]. THC was not found to influence the strength of either of these gPDMs ($P = .76$, $P = .60$; Fig. S6). The second feedforward gPDM which is characterized by sustained and oscillatory excitation was found to have a strong theta peak in the frequency domain. Furthermore, it was found that THC-induced declines in the strength of this gPDM were correlated with behavioral deficits ($R^2 = .30$, $P = .032$; Fig. 4c).

The three obtained feedback gPDMs are shown in Fig. 4b. These gPDMs express the essential feedback dynamics found in CA1 neurons. As previously mentioned, these dynamics arise through the combination of intracellular processes such as the AHP and extracellular processes such as recurrent connections between CA1 pyramidal cells and interneurons. It was found that THC-induced increases in the third feedback gPDM were correlated with behavioral deficits ($R^2 = .39$, $P = .005$; Fig. 4d). This correlation was not seen in either of the first two feedback gPDMs ($P = .32$, $P = .75$; Fig. S6). Notably, the 3rd feedback gPDM was seen to be "theta-blocking" in the frequency domain due to its trough at 8 Hz. This gPDM counteracts the 1st "theta-promoting" feedback gPDM and disrupts theta oscillations in the CA1 neuron. The THC-induced changes in the feedforward and feedback theta gPDMs paint a more complete picture of the CA1 theta reductions seen in Fig. 1e. Namely, they attribute the theta losses to specific feedforward and feedback dynamical filters which may potentially be

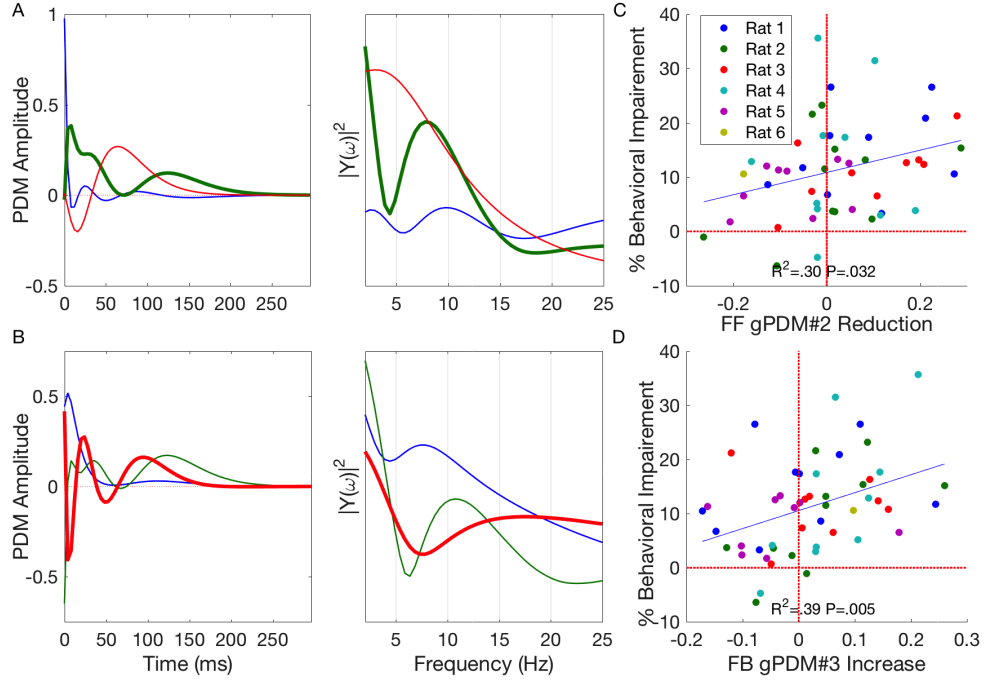


Figure 4: Feedforward (A) and feedback (B) global principal dynamic modes (gPDMs) in both the time (left) and frequency domain (right). Reductions in 2nd feedforward gPDM (C) and increases in 3rd feedback gPDM (D) were found to be correlated with behavioral deficits. Same format as Fig. 3.

traced to specific biophysical mechanisms. Furthermore, changes in these dynamical filters have been specifically correlated with behavioral deficits, which could not be done with theta reductions in the CA1 signal (Fig. S3).

3 Discussion

The current study uses 'data-driven' nonparametric system dynamics modeling tools to study the effects of THC on the Schaffer Collateral synapse in rodents. The chief findings of the study can be summarized as: (1) THC induced little or no change in traditional rate and temporal coding metrics such as MFR and theta power, (2) THC altered the CA1 excitatory-inhibitory balance by reducing feedforward influence from CA3 while increasing feedback excitation from CA1, (3) THC reduced theta information flow through the Schaffer collateral synapse, and (4) The magnitudes of both of the previous effects were directly correlated with the severity of behavioral deficits induced by THC. Overall these results suggest the conclusion that THC impairs memory encoding by functionally isolating CA1 from CA3.

From a computational perspective, the nonparametric modeling methods used in this study proved successful in studying the network level effects of cannabinoids since, unlike biophysical models, all model parameters were estimated directly from recorded data and very few *a priori* assumptions were

278 made about the effects of THC [19, 20, 51]. The global principal dynamic modes
279 (gPDMs), which were derived from MVAR filters of the entire population of neu-
280 rons, further extracted hidden dynamical structure from 'noisy' neuron-neuron
281 variability. Importantly, THC-induced changes in the gPDMs were directly cor-
282 related with behavioral impairments, thus justifying their utility. Furthermore,
283 while most in-vivo studies on THC analyze macro level signals such as ECoG
284 and EEG, this work adds to a relatively small body of literature which ana-
285 lyzes the effects of THC on neuronal population spiking activity. Finally, to our
286 knowledge, this is the first work which examines the effect of THC on neuronal
287 systems dynamics, or the causal interactions between signals, rather than on
288 neuronal signals themselves.

289 It was found that THC increased feedback excitatory index in CA1 and that
290 the magnitude of this effect was correlated with behavioral deficits. We hypoth-
291 esize that this is due to reduced feedback inhibition from CA1 cholecystokinin
292 (CCK)-containing cells. While CCK cells only make up only 13.9% of interneu-
293 rons [52], they express significantly more CB1 receptors than any other cell in
294 the hippocampus [53], and their primary output is to CA1 pyramidal cells [52].
295 Increased THC concentrations would reduce CCK interneuron output by (1) re-
296 ducing the amount of GABA they release per action potential (2) reducing their
297 MFR due to reduced glutamatergic input from principal cells in both CA3 and
298 CA1 [54, 55].

299 It was also found that THC reduced the number of casually connected CA3-
300 CA1 neuronal pairs; furthermore there was an interesting but insignificant trend
301 for THC-induced deficits in feedforward excitation to lead to behavioral deficits.
302 This trend may prove to be significant given a higher sample size. We hypoth-
303 esize that this reduced feedforward influence is caused by decreased glutamate
304 release from CA3 pyramidal cells due to CB1 receptor activation by THC [56].
305 Even though pyramidal cells have much lower densities of CB1 receptors than
306 interneurons [53, 57], there is evidence that CB induced reduction of excita-
307 tion is larger than these relative densities suggest. Principal cells outnumber
308 interneurons 20:1 in CA1 [50] and their CB1 receptors were found to be several
309 fold more efficacious than those of interneurons [58]. Further, lower baseline ac-
310 tivation levels of CB1 receptors on principal cells than on interneurons suggest
311 they would be disproportionately activated by CB agonists [59]. Altogether, the
312 decreased feedback inhibition and feedforward excitation amount to a functional
313 isolation, or breakdown in information flow between CA3 and CA1. We suggest
314 that this functional isolation is responsible for the behavioral impairments seen
315 in the DNMS task.

316 The 'functional isolation' hypothesis is further supported by previous work
317 which showed that the behavioral impairments caused by cannabinoids in the
318 DNMS task were similar to those seen with a full pharmacological lesion of the
319 hippocampus [60] Given the centrality of CA3→CA1 information flow to hip-
320 pocampal function, a functional isolation of these areas could indeed presumably
321 lead to impairments similar to that of a full lesion. Relatedly, Goonawardena
322 et al. [25] injected THC intraperitoneally at low 1 mg/kg doses as in this study
323 and in higher doses of 3 mg/kg. They found that while both doses disrupted

hippocampal synchrony, only the higher dose resulted in a reduction in pyramidal cell MFR. This suggests that at the lower dose both previously described phenomena are at a net balance, while at the higher dose, the decrease in feedforward excitation overpowers the increase in feedback excitation and results in lower MFR. Finally, the hypothesis predicts a breakdown in the normal spike-time coordination between pyramidal cells and interneurons in CA1 circuits. The breakdown of this coordination, which has been extensively implicated in hippocampal oscillations [61, 62], could be responsible for the observed decrease in theta oscillations and information flow.

Although the current results only suggest this hypothesis, several experiments could be done to further substantiate it. Feedforward and feedback kernels and gPDMs could be estimated at different doses of THC; the hypothesis would predict that different doses would effect the two processes independently, with one of the two processes potentially being more dominant at different THC levels. Significant developments in in-vivo synaptic patch clamping [63] and calcium imaging in recent years could be used to directly measure the drive of CCK cells and CA3 pyramidal cells onto CA1 pyramidal cells under THC.

Much research has been done investigating the effects THC and other cannabinoids have on seizures and epilepsy. Results so far have been mixed, with various studies showing that THC is both pro- and anticonvulsant [3, 4, 5, 6, 7, 8, 7]. The results from this study and the presented hypothesis suggest that THC inherently is not pro- or anti-convulsant but that its effects will depend on the dosage and the unique circuitry of every epileptic focus. Interestingly, a study by Rudenko et al. [6] has shown that indeed the effects of a CB1 agonist were dose dependant, with *lower* doses being anticonvulsant and higher doses being proconvulsant. Finally, this study suggests that in order to truly understand the effects of THC on epileptic circuits, one must study the systems level changes in circuit dynamics rather than taking a reductionist approach and studying the effects of THC on any particular receptor or cell type.

The present study analyzed the effects of THC from both a signals and systems perspective - and found that systems analysis yielded much richer results. For example, while analysis of CA1 spiketrain signals showed a slight (2%) reduction in theta frequency, analysis of system kernels showed that the theta loss was primarily due to CA1 feedback dynamics whose kernels lost over 20% of their theta power, while theta power in feedforward kernels was unaffected. Furthermore, only systems analysis allows one to analyze predictive power, feedforward and feedback excitation, and EPSP and AHP waveform shape. Notably, the finding that feedforward influence decreased while feedback excitation increased could not have been observed using only signal analysis which would have only detected a constant MFR.

The present study also employed gPDMs as a means to extract the most significant information from the kernel dynamics estimated from several animals over several sessions [19, 64, 18, 48]. The utility of the gPDM method was justified by the finding that reductions in theta related gPDMs in a given session were directly correlated with behavioral deficits, showing that the gPDMs can isolate the particular dynamics which are most affected by THC. Furthermore, THC-

370 induced theta power losses in spiketrain signals were not found to be correlated
371 with behavioral deficits. Although in the present study, kernels and gPDMs were
372 restricted to being linear in order to more easily quantify their overall strength
373 and excitation (via the EI), future work will aim to identify the effects of THC
374 on hippocampal nonlinear dynamics [65, 51].

375 Ethics Statement

376 All animal protocols were approved by the Wake Forest University Institutional
377 Animal Care and Use Committee, in accordance with the Association for Assess-
378 ment and Accreditation of Laboratory Animal Care and the National Institute
379 of Health Guide for the Care and Use of Laboratory Animals (NIH Publication
380 No. 8023).

381 Acknowledgements

382 This work was supported by NIH (www.nih.gov) grant P41-EB001978 to the
383 Biomedical Simulations Resource at the University of Southern California.

384 4 Methods

385 4.1 Experimental Procedures

386 N=6 Male Long-Evans rats were trained to criterion on a two lever, spatial
387 Delayed NonMatch-to-Sample (DNMS) task (see Fig. S1). Briefly, during the
388 sample phase the rat was presented one of two levers (left or right). After a delay
389 phase ranging from 1-30 seconds, the rat was presented both levers and had to
390 choose the opposite level in order to attain a reward. Each rodent underwent 16-
391 25 sessions of the task, which were roughly evenly divided between control and
392 THC sessions, wherein the rodent was intraperitoneally administered 1 mg/kg of
393 body weight Δ^9 -tetrahydrocannabinol (THC), an exogenous cannabinoid found
394 in marijuana. During the task, spike trains were recorded in-vivo with multi-
395 electrode arrays implanted in the left and right CA3 and CA1 regions of the
396 hippocampus. In an effort to acquire a consistent cognitive state, only spiking
397 activity around the sample phase of the task was used. Spikes from multiple
398 trials were sorted, time-stamped, and concatenated into a discretized binary
399 time series using a 4ms bin. For more details on the experimental setup, see
400 supplementary methods.

401 4.2 Model Configuration and Estimation

402 Nonparametric multiple-input linear autoregressive models were used to model
403 the dynamical transformation between input and output spike trains (see Fig.
404 2,5) [18, 51]. Each model consisted of a feedforward component, reflecting the
405 effect of the N input cells on the output cell and a feedback (autoregressive)

406 component reflecting the subthreshold and suprathreshold effects the output
 407 cell has on itself. Thus, the output $y(t)$ is calculated as:

$$y(t) = \sum_{n=1}^N \sum_{\tau=0}^M k_n(\tau) x_n(t - \tau) + \sum_{\tau=1}^{M+1} k_{AR}(\tau) y(t - \tau) \quad (1)$$

408 where k_n reflects the feedforward filter of input $x_n(t)$, and k_{AR} reflects the feed-
 409 back filter. In order to reduce the number of model parameters and thereby
 410 increase parameter stability, we applied the Laguerre expansion technique to ex-
 411 pand the feedforward and feedback filters over L Laguerre basis functions (see
 412 supplementary methods).

413 Effective connectivity between neurons was assessed using a Granger causality-
 414 like approach. For each output CA1 neuron, input CA3 neurons were selected
 415 in a forward stepwise procedure whereby only neurons which help predict the
 416 output CA1 spike activity were included in the model. After all input neurons
 417 were selected, a Monte Carlo approach was used to assess model significance. A
 418 model was deemed significant if the CA3 inputs could predict the output CA1
 419 activity significantly better ($P < .0001$) than randomly permuted versions of the
 420 inputs. See supplementary methods for more details.

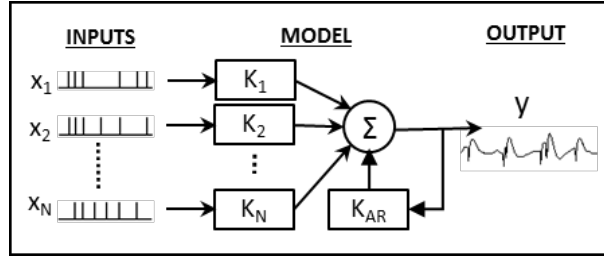


Figure 5: Model Configuration. Each model has N point-process inputs which each go through a linear filter, K_i . These inputs are then summed with the output of the feedback filter, K_{AR} to generate the final output, $y(t)$, which is a continuous signal

421 4.3 Principal Dynamic Modes

422 The global principal dynamic modes (gPDMs) were obtained in a two step pro-
 423 cess: first, all filters of each input from every animal were concatenated in a
 424 rectangular matrix. Then singular value decomposition (SVD) was performed
 425 on the rectangular matrix to obtain all the significant singular vectors, which
 426 are the gPDMs. It was found that 3 gPDMs were sufficient to describe the lin-
 427 ear dynamics both the population of feedforward and feedback filters. gPDM
 428 strength in a given filter was computed by taking the dot product between the
 429 gPDM and the filter. gPDM strength in a given session was computed by taking
 430 the average gPDM strength in every filter of that session.

431 **A Supplementary Methods**

432 All data was previously used in a study on the effects of cannabinoids on hip-
433 pocampal multifractality [21, 22])

434 **A.1 Animals**

435 Subjects were Long–Evans rats (Harlan) aged 4–6 months ($n = 6$) individually
436 housed and allowed free access to food with water regulation to maintain 85% of
437 ad libitum body weight during testing. All animal protocols were approved by
438 the Wake Forest University Institutional Animal Care and Use Committee, in
439 accordance with the Association for Assessment and Accreditation of Laboratory
440 Animal Care and the National Institute of Health Guide for the Care and Use
441 of Laboratory Animals (NIH Publication No. 8023).

442 **A.2 Apparatus**

443 The behavioral testing apparatus for the delayed nonmatch-to-sample (DNMS)
444 task is the same as reported in other studies [23] and consisted of a 43x43x50 cm
445 Plexiglas chamber with two retractable levers (left and right) positioned on either
446 side of a water trough on the front panel. A nosepoke device (photocell) was
447 mounted in the center of the wall opposite the levers with a cue light positioned
448 immediately above the nosepoke device. A video camera was mounted on the
449 ceiling and the entire chamber was housed inside a commercially built sound-
450 attenuated cubicle.

451 **A.3 DNMS Task**

452 The DNMS task consisted of three main phases: Sample, Delay and Nonmatch.
453 The sample phase initiated the trial when either the left or right lever was
454 extended (50% probability), requiring the animal to press it as the Sample Re-
455 sponse (SR). The lever was then retracted and the Delay phase of the task
456 initiated, as signaled by the illumination of a cue light over the nosepoke pho-
457 tocell device on the wall on the opposite side of the chamber. At least one
458 nosepoke (NP) was required following the delay interval which varied randomly
459 in duration (1-30 s) on each trial during the session. The Nonmatch phase began
460 when the delay timed out, the photocell cue light turned off and both the left
461 and right levers on the front panel were extended. Correct responses consisted
462 of pressing the lever in the Nonmatch phase located in the spatial position op-
463 posite the SR (nonmatch response: NR). This produced a drop of water (0.4
464 ml) reward in the trough between the two levers. After the NR the levers were
465 retracted for a 10.0 second intertrial interval (ITI) before the next Sample lever
466 was presented to begin the next trial. A lever press at the same position as the
467 SR (match response) constituted an “error” with no water delivery and turned
468 off of the chamber house lights for 5.0s and the next trial was presented 5.0 s
469 later. Individual performance was assessed as % NRs (correct responses) with
470 respect to the total number of trials (80-100) per daily (1 hr) sessions.

471 A.4 Drug Preparation & Administration

472 Δ^9 -tetrahydrocannabinol (THC) was obtained from the National Institute on
473 Drug Abuse as a 50 mg/ml solution in ethanol. Detergent vehicle was pre-
474 pared from Pluronic F68 (Sigma, St. Louis, MO), 20 mg/ml in ethanol. THC
475 was added to the detergent-ethanol solution (0.5 ml of either THC), and then 2.0
476 ml of saline (0.9%) was slowly added to the ethanol-drug solution. The solution
477 was stirred rapidly and placed under a steady stream of nitrogen gas to evapo-
478 rate the ethanol (~ 10 min). This resulted in a detergent-drug suspension (12.5
479 mg/ml THC), which was sonicated and then diluted with saline to final injec-
480 tion concentrations (0.5-2.0 mg/ml THC). On drug administration days, animals
481 were injected intraperitoneally with the drug-detergent solution (1 mg/kg) ~ 10
482 min before the start of the behavioral session. Our experience with these ex-
483 periments has shown that performance after vehicle injection is not significantly
484 different than no injection, and therefore was omitted during this series of ex-
485 periments to minimize risk of infection to the animals. At least two no injection
486 days were imposed between each drug-testing session. All drug solutions were
487 mixed fresh each day.

488 A.5 Surgery

489 All surgical procedures conformed to National Institutes of Health and Associ-
490 ation for Assessment and Accreditation of Laboratory Animal Care guidelines,
491 and were performed in a rodent surgical facility approved by the Wake Forest
492 University Institutional Animal Care and Use Committee. After being trained to
493 criterion performance level in the DNMS task animals were anesthetized with ke-
494 tamine (100 mg/kg) and xylazine (10 mg/kg) and placed in a stereotaxic frame.
495 Craniotomies (5mm-diameter) were performed bilaterally over the dorsal hip-
496 pocampus to provide for implantation of 2 identical array electrodes (Neurolinec,
497 New York, NY), each consisting of two rows of 8 stainless steel wires (diameter:
498 20 μm) positioned such that the geometric center of each electrode array was
499 centered at co-ordinates 3.4 mm posterior to Bregma and 3.0 mm lateral (right
500 or left) to midline [66]. The array was designed such that the distance between
501 two adjacent electrodes within a row was 200 μm and between rows was 400
502 μm to conform to the locations of the respective CA3 and CA1 cell layers. The
503 longitudinal axis of the array of electrodes was angled 30° to the midline during
504 implantation to conform to the orientation of the longitudinal axis of the hip-
505 pocampus, with posterior electrode sites more lateral than anterior sites. The
506 electrode array was lowered in 25-100 μm steps to a depth of 3.0 - 4.0 mm from
507 the cortical surface for the longer electrodes positioned in the CA3 cell layer,
508 leaving the shorter CA1 electrodes 1.2 mm higher with tips in the CA1 layer.
509 Extracellular neuronal spike activity was monitored from all electrodes during
510 surgery to maximize placement in the appropriate hippocampal cell layers. After
511 placement of the array the cranium was sealed with bone wax and dental cement
512 and the animals treated with buprenorphine (0.01–0.05 mg/kg) for pain relief
513 over the next 4-6 hrs. The scalp wound was treated periodically with Neosporin
514 antibiotic and systemic injections of penicillin G (300,000 U, intramuscular) were

515 given to prevent infection. Animals were allowed to recover from surgery for at
516 least 1 week before continuing behavioral testing [67].

517 **A.6 Electrophysiological Monitoring & Preprocessing**

518 Animals were connected by cable to the recording apparatus via a 32-channel
519 headstage and harness attached to a 40-channel slip-ring commutator (Crist
520 Instruments, Hagerstown, MD) to allow free movement in the behavioral test-
521 ing chamber. Single neuron action potentials (spikes) were isolated by time-
522 amplitude window discrimination and computer-identified individual waveform
523 characteristics using a multi-neuron acquisition (MAP) processor (Plexon Inc.,
524 Dallas, TX, USA). Single neuron spikes were recorded daily and identified us-
525 ing waveform and firing characteristics within the task (perievent histograms)
526 for each of the DNMS events (SR, LNP & NR). To maintain waveform shape
527 across days, all recorded data was concatenated into one file (separately for each
528 rat) and offline sorting was performed using principal component analysis, peak-
529 valley, and nonlinear energy algorithms in Offline Sorter (Plexon Inc., Dallas,
530 TX, USA). Hippocampal neuron ensembles used to distinguish recording phases
531 and drug treatment conditions consisted of 10-30 single neurons, each recorded
532 from a separate identified electrode location on either of the bilateral arrays.
533 All isolated spike trains contained no less than a 1 ms gap at the center of the
534 autocorrelogram. No effort was made to differentiate between principal cells and
535 interneurons. Previous work has shown that hippocampal neurons recorded with
536 the same waveform from the same electrodes exhibit consistent mean, baseline
537 and DNMS task modulated firing rate alterations [68, 26], and therefore indi-
538 vidual neurons were treated as the same when recorded over multiple days. A
539 total of 189 neurons recorded during 5,143 recording phases were analyzed in
540 the reported experiments.

541 **A.7 Sample-Response Cell Identification**

542 Prior studies from this laboratory have identified hippocampal neurons recorded
543 as above by “Functional Cell Types” (FCTs) described by different behavioral
544 correlates of DNMS task-related events such as lever position and/or phase of
545 the task [26, 25]. Sample-response cells, a subtype of FCTs, were identified by
546 first constructing a smoothed (51 bin) perievent histogram around the sample
547 presentation phase of the DNMS task. The neurons background firing rate mean
548 and variance were calculated from activity 3.5-5s after sample presentation. If
549 the neuron’s MFR from the 2 second window around sample presentation was
550 4 standard deviations greater than its MFR from the background period it was
551 classified as a sample-response cell. It should be noted that for the purpose of
552 this paper other FCTs such as those which respond to a specific lever (left/right)
553 or trial-type cells were not considered [69].

554 A.8 Laguerre Expansion Technique

555 In order to apply the Laguerre expansion technique [19], the input and output
556 data records were first convolved with the Laguerre functions:

$$v_{x_i}^{(l)} = \sum_{\tau=0}^M b_l(\tau) x_i(t - \tau) \quad (2)$$

557

$$v_y^{(l)} = \sum_{\tau=0}^M b_l(\tau) y(t - \tau) \quad (3)$$

558 where b_l is the l^{th} Laguerre basis function. By first convolving with the Laguerre
559 basis functions, the dynamical effects of the past input epochs are removed and
560 we are left with a simple regression of contemporaneous data. Substituting the
561 above equations into equation 1, we have:

$$y(t) = k_0 + \sum_{n=1}^N \sum_{l=1}^L c_{l,x_i}(l) v_{l,x_i}(t) + \sum_{l=1}^L c_{l,y}(l) v_{l,y}(t) \quad (4)$$

562 where c_{l,x_i} and $c_{l,y}$ are the feedforward and feedback Laguerre expansion coeffi-
563 cients. To estimate model parameters, eq. 4 was cast in matrix form:

$$\mathbf{y} = \mathbf{V}\mathbf{c} + \epsilon \quad (5)$$

564 where \mathbf{y} is the vector of all N output samples, \mathbf{V} is the design matrix consisting
565 of the convolved inputs, \mathbf{c} are the model parameters to be estimated, and ϵ is
566 the modeling error. Eq. 5 was solved using least squares regression (LSR). The
567 memory of our system was fixed at 300ms, in accordance with previous studies
568 [65, 70]. The Laguerre parameter α was fixed at 0.6 to reflect this system memory
569 [19].

570 A.9 Model Selection

571 In theory, the most predictive model would include all recorded inputs. However,
572 such a model would be susceptible to overfitting, and would not reveal which
573 neurons are causally connected to each other. To overcome this issue a forward
574 step-wise selection procedure was used to minimize overfitting and prune out
575 all inputs which are not causally related to the output [71]. Given an output
576 cell and M potential input cells recorded during the same session, the following
577 steps were used to select the N input cells which are causally connected to the
578 output cell. First, the data was divided into training (in-sample) and testing
579 (out-of-sample) sets. Then, M single-input single-output (SISO) models were
580 constructed with each of the potential inputs. The model whose predicted output
581 had the highest correlation, as measured by the Pearson correlation-coefficient,
582 ρ , with the actual output was selected. Afterwards, $N-1$ models were constructed
583 with two inputs: the previously selected input and one of the remaining potential
584 inputs. If any of the inputs were able to raise ρ , the input which raised ρ the

most was selected; otherwise, the procedure was ended, and only 1 input was selected. This procedure was repeated until either none of the inputs were able to raise ρ , or all M potential neurons were selected. The N selected neurons were then used as the model input.

A.10 Model Validation

To avoid overfitting, Monte Carlo style simulations were used to select those models which represent significant causal connections between input and output neurons and do not just fit noise [72]. The following procedure was used: in each run the real input was randomly permuted with respect to the output. A model was then generated between the permuted input and the real output, and the Pearson correlation coefficient, ρ_i , was obtained as a metric of performance. T=40 such simulations were conducted for each output and a set of performance metrics, $\{\rho_i\}_i^T$, was obtained. Then, using Fisher's transformation, we tested the hypothesis, H_0 , that ρ was within the population of $\{\rho_i\}$. If this hypothesis could be rejected at the 99.99% significance level, the model was deemed significant. The very conservative threshold ($P < .0001$) was used due to the large number of comparisons being made.

A.11 Statistical Analysis

Unless otherwise noted, the unpaired Mann-Whitney U test was used to access whether significant differences exist between two samples. This test was used since it does not assume a normal distribution, and much of our data was found to be skewed/nonnormal. Shift estimates (Hodges-Lehman) and confidence intervals were estimated as prescribed by Higgins [73]. In order to estimate the scale estimate, or the ratio between two samples, the data was first log-transformed and then scale estimate was taken to be the antilog of the shift estimate. The χ^2 test was used to compare proportions.

In addition to the Pearson correlation coefficient, ρ , Receiver Operating Characteristic (ROC) curves were used to visualize model performance. ROC curves plot the true positive rate against the false positive rate over the putative range of threshold values for the continuous output, y [72]. The area under the curve (AUC) of ROC plots are used as a performance metric of the model, and have been shown to be equivalent to the Mann-Whitney two sample statistic [74]. The AUC ranges from 0 to 1, with 0.5 indicating a random predictor and higher values indicating better model performance. The ρ and AUC metrics were chosen as they measure the similarity between a continuous 'prethreshold' signal and a spike train. The continuous 'prethreshold' signal was chosen over adding a threshold trigger and comparing true output spike train with an output 'post-threshold' spike train for two reasons. First, this allows us to avoid specifying the threshold trigger value, which relies on the somewhat arbitrary tradeoff between true-positive and false-negative spikes [45]. Also, similarity metrics between two spike trains often require the specification of a 'binning parameter' to determine

626 the temporal resolution of the metric [75, 76].¹

627 B Supplementary Figures

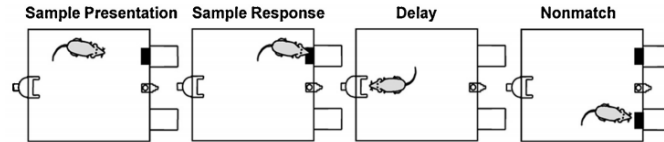


Figure S1: Schematic of the DNMS task. First the rat is presented with one of two levers (sample presentation), which it presses (sample response). Then following a delay phase, the rat is presented with both levers (Nonmatch), of which it must press the opposite level from which it was presented in order to successfully complete the task.

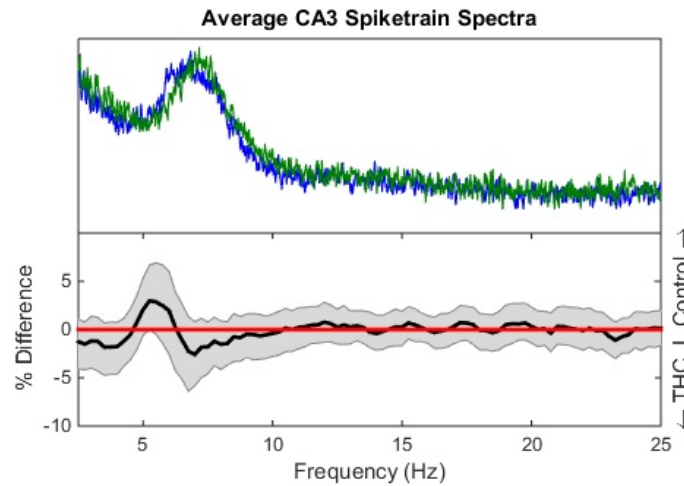


Figure S2: CA3 spectra mean frequency and differences. Same format as Fig. 1e. A weak but significant trend was found for declining CA3 theta oscillations ($\Delta = 1.94\%$, $P = .045$).

¹I should probably add sections on how behavioral correlation analysis & FFT was done...

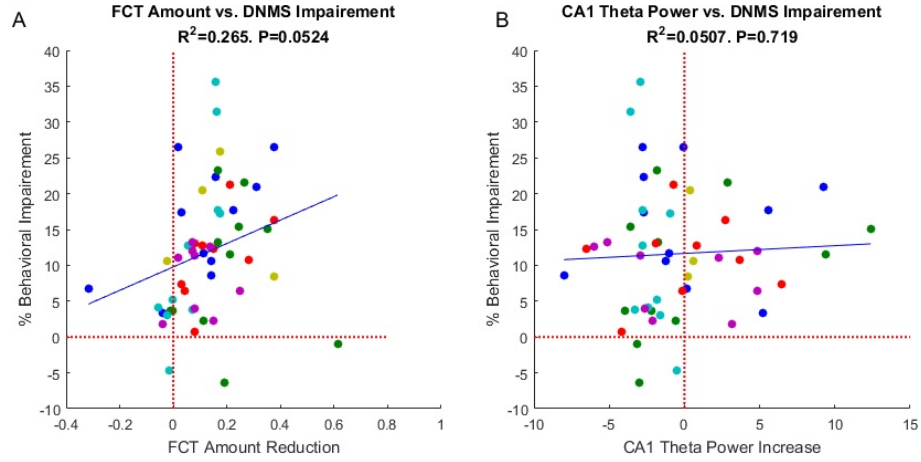


Figure S3: (A) A suggestive but insignificant relationship was found between the THC-induced decrease in the mean number of sample-presentation cells and behavioral performance ($R^2 = .265$, $P = .052$). (B) No relationship was found between reductions in CA1 theta power and behavioral impairment ($P = .67$). Format is same as Fig. 3.

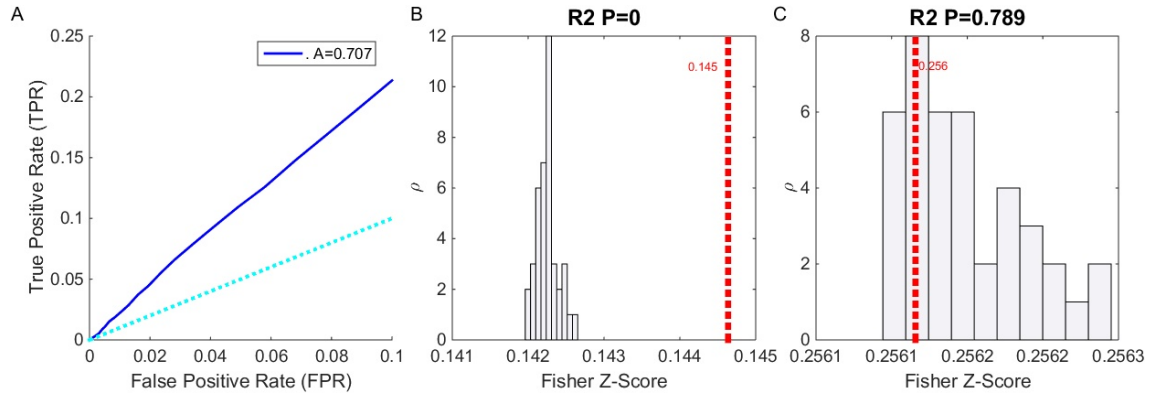


Figure S4: (A) ROC plot (see supplementary methods) for model shown in Fig. 2 showing model predictive power. The light blue line ($TPR=FPR$) indicates a model with no predictive power. (B,C) Examples of Monte Carlo simulations: For each model, 40 surrogate models with shuffled inputs were generated. The Fisher z-scores of these models, which are derived from ρ , were plotted as a histogram, while the true ρ value is the plotted dashed red line. The P value for the hypothesis that the true ρ value is greater than the simulated ρ values is printed above the graphs. Models were deemed significant if $P < .0001$. (B) shows the results for the model in Fig. 2, which was deemed significant. (C) shows an insignificant model

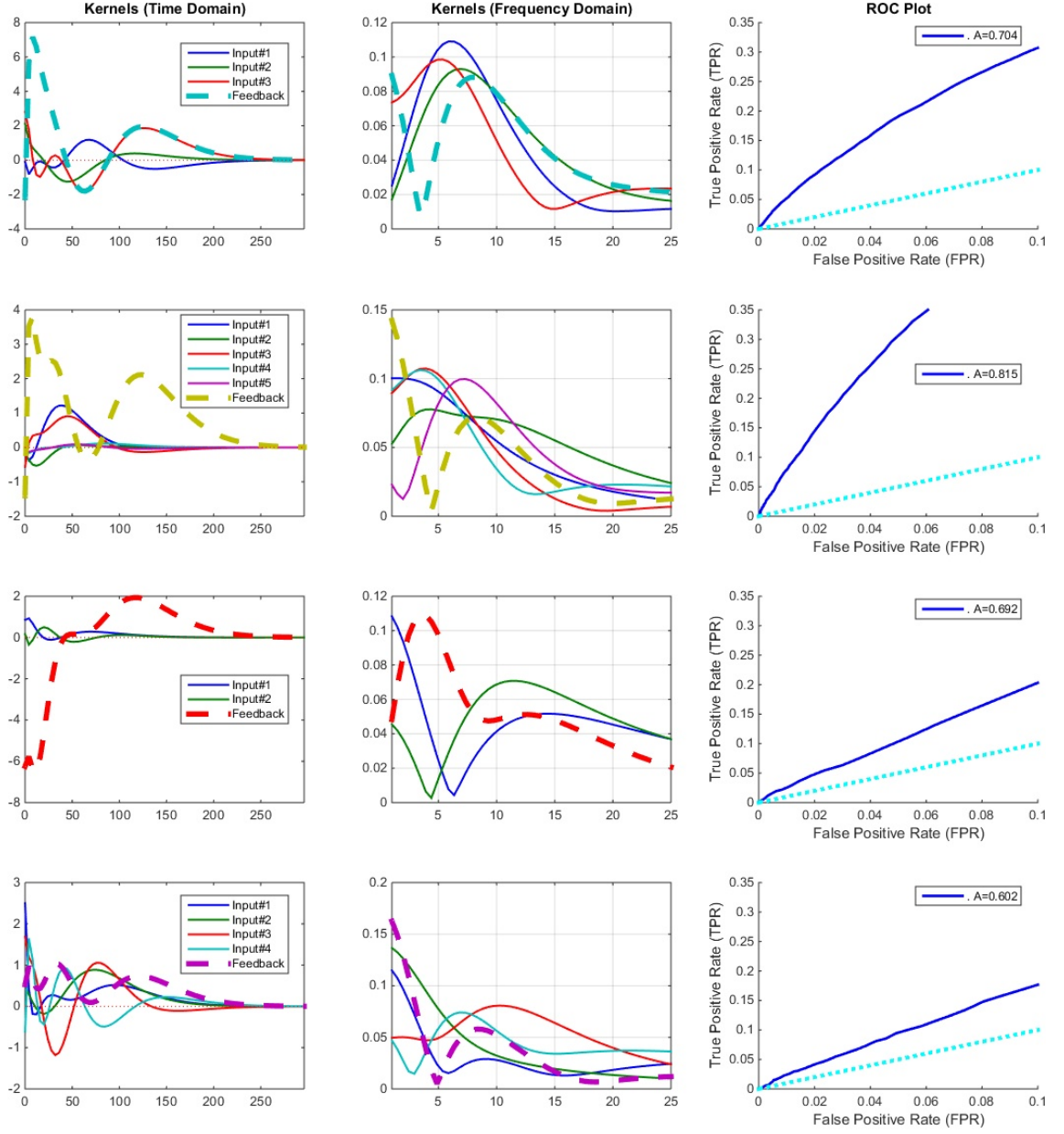


Figure S5: 4 additional systems are presented. Left column shows all system filters, including feedback filter (dashed line) in the time domain. Middle column shows the filters in the frequency domain and right column shows the ROC plots of the models. All these models were found to have significant predictive power in Monte Carlo tests.

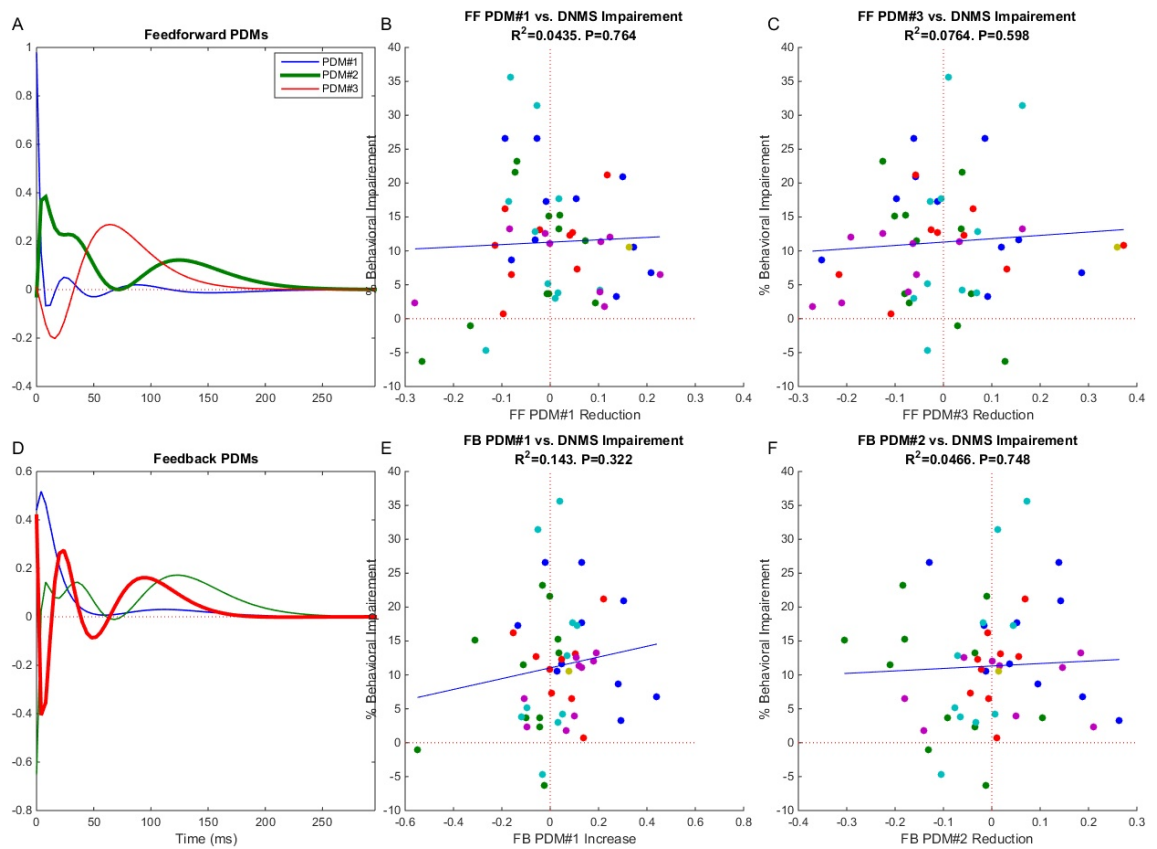


Figure S6: Top Row: neither the first (middle column) nor third feedforward gPDM were found to be significantly correlated with THC induced behavioral deficits. Bottom Row: neither the first (middle column) nor second feedback gPDM were found to be significantly correlated with THC induced behavioral deficits. Format is same as Fig. 3.

References

- [1] Barbara S Koppel, John CM Brust, Terry Fife, Jeff Bronstein, Sarah Youssof, Gary Gronseth, and David Gloss. Systematic review: Efficacy and safety of medical marijuana in selected neurologic disorders report of the guideline development subcommittee of the american academy of neurology. *Neurology*, 82(17):1556–1563, 2014.
- [2] Liana Fattore. *Cannabinoids in Neurologic and Mental Disease*. Academic Press, 2015.
- [3] Melisa J Wallace, Jenny L Wiley, Billy R Martin, and Robert J DeLorenzo. Assessment of the role of cb 1 receptors in cannabinoid anticonvulsant effects. *European Journal of Pharmacology*, 428(1):51–57, 2001.
- [4] Robert E Blair, Laxmikant S Deshpande, Sompong Sombati, Katherine W Falenski, Billy R Martin, and Robert J DeLorenzo. Activation of the cannabinoid type-1 receptor mediates the anticonvulsant properties of cannabinoids in the hippocampal neuronal culture models of acquired epilepsy and status epilepticus. *Journal of Pharmacology and Experimental Therapeutics*, 317(3):1072–1078, 2006.
- [5] Laxmikant S Deshpande, Sompong Sombati, Robert E Blair, Dawn S Carter, Billy R Martin, and Robert J DeLorenzo. Cannabinoid cb1 receptor antagonists cause status epilepticus-like activity in the hippocampal neuronal culture model of acquired epilepsy. *Neuroscience letters*, 411(1):11–16, 2007.
- [6] V Rudenko, A Rafiuddin, JR Lehesté, and LK Friedman. Inverse relationship of cannabimimetic (r+) win 55, 212 on behavior and seizure threshold during the juvenile period. *Pharmacology Biochemistry and Behavior*, 100(3):474–484, 2012.
- [7] István Katona. Cannabis and endocannabinoid signaling in epilepsy. In *Endocannabinoids*, pages 285–316. Springer, 2015.
- [8] Andrew J Hill, TD Hill, and B Whalley. The development of cannabinoid based therapies for epilepsy. *Endocannabinoids: molecular, pharmacological, behavioral and clinical features*. bentham science publishers, Oak Park, IL, pages 164–204, 2013.
- [9] Raphael Mechoulam, Lumír O Hanuš, Roger Pertwee, and Allyn C Howlett. Early phytocannabinoid chemistry to endocannabinoids and beyond. *Nature Reviews Neuroscience*, 2014.
- [10] Emma Puighermanal, Arnau Busquets-Garcia, Rafael Maldonado, and Andrés Ozaita. Cellular and intracellular mechanisms involved in the cognitive impairment of cannabinoids. *Philosophical Transactions of the Royal Society B: Biological Sciences*, 367(1607):3254–3263, 2012.

- 667 [11] Mathilde Metna-Laurent and Giovanni Marsicano. Rising stars: Modulation
668 of brain functions by astroglial type-1 cannabinoid receptors. *Glia*, 63(3):
669 353–364, 2015.
- 670 [12] Giovanni Bénard, Federico Massa, Nagore Puente, Joana Lourenço, Luigi
671 Bellocchio, Edgar Soria-Gómez, Isabel Matias, Anna Delamarre, Mathilde
672 Metna-Laurent, Astrid Cannich, et al. Mitochondrial cb1 receptors regulate
673 neuronal energy metabolism. *Nature Neuroscience*, 15(4):558–564, 2012.
- 674 [13] Wei Xiong, KeJun Cheng, Tanxing Cui, Grzegorz Godlewski, Kenner C
675 Rice, Yan Xu, and Li Zhang. Cannabinoid potentiation of glycine receptors
676 contributes to cannabis-induced analgesia. *Nature Chemical Biology*, 7(5):
677 296–303, 2011.
- 678 [14] Jessica A Fawley, Mackenzie E Hofmann, and Michael C Andresen.
679 Cannabinoid 1 and transient receptor potential vanilloid 1 receptors dis-
680 cretely modulate evoked glutamate separately from spontaneous glutamate
681 transmission. *The Journal of Neuroscience*, 34(24):8324–8332, 2014.
- 682 [15] Stephanie C Gantz and Bruce P Bean. Cell-autonomous excitation of
683 midbrain dopamine neurons by endocannabinoid-dependent lipid signaling.
684 *Neuron*, 2017.
- 685 [16] Moyra A Coull, Andrew T Johnston, Roger G Pertwee, and Stephen N
686 Davies. Action of δ -9-tetrahydrocannabinol on gaba a receptor-mediated
687 responses in a grease-gap recording preparation of the rat hippocampal slice.
688 *Neuropharmacology*, 36(10):1387–1392, 1997.
- 689 [17] Timothy M Brown, Jonathan M Brotchie, and Stephen M Fitzjohn.
690 Cannabinoids decrease corticostriatal synaptic transmission via an effect
691 on glutamate uptake. *The Journal of Neuroscience*, 23(35):11073–11077,
692 2003.
- 693 [18] Roman A Sandler, Dong Song, Robert E Hampson, Sam A Deadwyler,
694 Theodore W Berger, and Vasilis Z Marmarelis. Model-based asesment of an
695 in-vivo predictive relationship from ca1 to ca3 in the rodent hippocampus.
696 *Journal of Computational Neuroscience*, pages 1–15, 2014.
- 697 [19] Vasilis Z Marmarelis. *Nonlinear dynamic modeling of physiological systems*.
698 Wiley-Interscience, 2004.
- 699 [20] Dong Song, Vasilis Z Marmarelis, and Theodore W Berger. Parametric and
700 non-parametric modeling of short-term synaptic plasticity. part i: Compu-
701 tational study. *Journal of Computational Neuroscience*, 26(1):1–19, 2009.
- 702 [21] Dustin Fetterhoff, Ioan Opris, Sean L Simpson, Sam A Deadwyler, Robert E
703 Hampson, and Robert A Kraft. Multifractal analysis of information pro-
704 cessing in hippocampal neural ensembles during working memory under δ
705 9-tetrahydrocannabinol administration. *Journal of Neuroscience Methods*,
706 2014.

- 707 [22] Dustin Fetterhoff, Robert A Kraft, Roman A Sandler, Ioan Opris, Cheryl A
708 Sexton, Vasilis Z Marmarelis, Robert E Hampson, and Sam A Deadwyler.
709 Distinguishing cognitive state with multifractal complexity of hippocampal
710 interspike interval sequences. *Frontiers in Systems Neuroscience*, 9, 2015.
- 711 [23] Robert E Hampson and Sam A Deadwyler. Cannabinoids reveal the neces-
712 sity of hippocampal neural encoding for short-term memory in rats. *The*
713 *Journal of Neuroscience*, 20(23):8932–8942, 2000.
- 714 [24] David Robbe, Sean M Montgomery, Alexander Thome, Pavel E Rueda-
715 Orozco, Bruce L McNaughton, and György Buzsáki. Cannabinoids reveal
716 importance of spike timing coordination in hippocampal function. *Nature*
717 *Neuroscience*, 9(12):1526–1533, 2006.
- 718 [25] Anushka V Goonawardena, Lianne Robinson, Robert E Hampson, and Ger-
719 not Riedel. Cannabinoid and cholinergic systems interact during perfor-
720 mance of a short-term memory task in the rat. *Learning & Memory*, 17
721 (10):502–511, 2010.
- 722 [26] Robert E Hampson, John D Simeral, and Sam A Deadwyler. Distribution
723 of spatial and nonspatial information in dorsal hippocampus. *Nature*, 402
724 (6762):610–614, 1999.
- 725 [27] David Robbe and György Buzsáki. Alteration of theta timescale dynamics
726 of hippocampal place cells by a cannabinoid is associated with memory
727 impairment. *The Journal of Neuroscience*, 29(40):12597–12605, 2009.
- 728 [28] Gyorgy Buzsaki. *Rhythms of the Brain*. Oxford University Press, 2006.
- 729 [29] Laura Lee Colgin. Mechanisms and functions of theta rhythms. *Annual*
730 *Review of Neuroscience*, 36:295–312, 2013.
- 731 [30] György Buzsáki and Edvard I Moser. Memory, navigation and theta rhythm
732 in the hippocampal-entorhinal system. *Nature Neuroscience*, 16(2):130–138,
733 2013.
- 734 [31] James M Hyman, Eric A Zilli, Amanda M Paley, and Michael E Hasselmo.
735 Working memory performance correlates with prefrontal-hippocampal theta
736 interactions but not with prefrontal neuron firing rates. *Frontiers in Inte-*
737 *grative Neuroscience*, 4, 2010.
- 738 [32] Mihály Hajós, William E Hoffmann, and Bernát Kocsis. Activation of
739 cannabinoid-1 receptors disrupts sensory gating and neuronal oscillation:
740 relevance to schizophrenia. *Biological psychiatry*, 63(11):1075–1083, 2008.
- 741 [33] N Spruston and C McBain. Structural and functional properties of hip-
742 pocampal neurons. *The Hippocampus Book*, pages 133–201, 2007.
- 743 [34] Thomas Klausberger and Peter Somogyi. Neuronal diversity and temporal
744 dynamics: the unity of hippocampal circuit operations. *Science*, 321(5885):
745 53–57, 2008.

- [35] Frédéric Pouille and Massimo Scanziani. Enforcement of temporal fidelity in pyramidal cells by somatic feed-forward inhibition. *Science*, 293(5532):1159–1163, 2001.
- [36] Rita Zemankovics, Judit M Veres, Iris Oren, and Norbert Hájos. Feedforward inhibition underlies the propagation of cholinergically induced gamma oscillations from hippocampal ca3 to ca1. *The Journal of Neuroscience*, 33(30):12337–12351, 2013.
- [37] L Stan Leung and Hui-Wen Yu. Theta-frequency resonance in hippocampal ca1 neurons in vitro demonstrated by sinusoidal current injection. *Journal of neurophysiology*, 79(3):1592–1596, 1998.
- [38] Bruce Hutcheon and Yosef Yarom. Resonance, oscillation and the intrinsic frequency preferences of neurons. *Trends in Neurosciences*, 23(5):216–222, 2000.
- [39] Bernat Kocsis, Anatol Bragin, and György Buzsáki. Interdependence of multiple theta generators in the hippocampus: a partial coherence analysis. *The Journal of neuroscience*, 19(14):6200–6212, 1999.
- [40] György Buzsáki. Theta oscillations in the hippocampus. *Neuron*, 33(3):325–340, 2002.
- [41] Romain Goutagny, Jesse Jackson, and Sylvain Williams. Self-generated theta oscillations in the hippocampus. *Nature Neuroscience*, 12(12), 2009.
- [42] Krisztina Monory, Martin Polack, Anita Remus, Beat Lutz, and Martin Korte. Cannabinoid cb1 receptor calibrates excitatory synaptic balance in the mouse hippocampus. *The Journal of Neuroscience*, 35(9):3842–3850, 2015.
- [43] SA Turkanis and R Karler. Central excitatory properties of δ 9-tetrahydrocannabinol and its metabolites in iron-induced epileptic rats. *Neuropharmacology*, 21(1):7–13, 1982.
- [44] Angela B Clement, E Gregory Hawkins, Aron H Lichtman, and Benjamin F Cravatt. Increased seizure susceptibility and proconvulsant activity of anandamide in mice lacking fatty acid amide hydrolase. *The Journal of Neuroscience*, 23(9):3916–3923, 2003.
- [45] Vasilis Z Marmarelis, Dae C Shin, Dong Song, Robert E Hampson, Sam A Deadwyler, and Theodore W Berger. Nonlinear modeling of dynamic interactions within neuronal ensembles using principal dynamic modes. *Journal of computational neuroscience*, 34(1):73–87, 2013.
- [46] Roman A Sandler and Vasilis Z. Marmarelis. Understanding spike triggered covariance using wiener theory for receptive field identification. *Journal of Vision*, in press.

- 784 [47] Sam A Deadwyler, James R West, Carl W Cotman, and Gary Lynch. Phys-
785 iological studies of the reciprocal connections between the hippocampus and
786 entorhinal cortex. *Experimental Neurology*, 49(1):35–57, 1975.
- 787 [48] Roman A Sandler, Dong Song, Robert E Hampson, Sam A Deadwyler,
788 Theodore W Berger, and Vasilis Z Marmarelis. Closed-loop hippocam-
789 pal modeling and the design of neurostimulation patterns for suppressing
790 seizures. *Journal of Neural Engineering*, Under Review.
- 791 [49] Roland SG Jones. Entorhinal-hippocampal connections: a speculative view
792 of their function. *Trends in Neurosciences*, 16(2):58–64, 1993.
- 793 [50] Omar J Ahmed and Mayank R Mehta. The hippocampal rate code:
794 anatomy, physiology and theory. *Trends in neurosciences*, 32(6):329–338,
795 2009.
- 796 [51] Roman A Sandler, Samuel A Deadwyler, Robert E Hampson, Dong Song,
797 Theodore W Berger, and Vasilis Z Marmarelis. System identification of
798 point-process neural systems using probability based volterra kernels. *Jour-
799 nal of Neuroscience Methods*, 240:179–192, 2015.
- 800 [52] Marianne J Bezaire and Ivan Soltesz. Quantitative assessment of cal lo-
801 cal circuits: Knowledge base for interneuron-pyramidal cell connectivity.
802 *Hippocampus*, 23(9):751–785, 2013.
- 803 [53] I Katona, B Sperlagh, Zs Maglóczy, E Santha, A Köfalvi, S Czirjak,
804 K Mackie, ES Vizi, and TF Freund. Gabaergic interneurons are the targets
805 of cannabinoid actions in the human hippocampus. *Neuroscience*, 100(4):
806 797–804, 2000.
- 807 [54] Ferenc Mátyás, Tamás F Freund, and Attila I Gulyás. Convergence of
808 excitatory and inhibitory inputs onto cck-containing basket cells in the cal
809 area of the rat hippocampus. *European Journal of Neuroscience*, 19(5):
810 1243–1256, 2004.
- 811 [55] Sang-Hun Lee, Csaba Földy, and Ivan Soltesz. Distinct endocannabinoid
812 control of gaba release at perisomatic and dendritic synapses in the hip-
813 pocampus. *Journal of Neuroscience*, 30(23):7993–8000, 2010.
- 814 [56] Maoxing Shen, Timothy M Piser, Virginia S Seybold, and Stanley A Thayer.
815 Cannabinoid receptor agonists inhibit glutamatergic synaptic transmission
816 in rat hippocampal cultures. *The Journal of Neuroscience*, 16(14):4322–
817 4334, 1996.
- 818 [57] Takako Ohno-Shosaku, Hiroshi Tsubokawa, Ichiro Mizushima, Norihide
819 Yoneda, Andreas Zimmer, and Masanobu Kano. Presynaptic cannabinoid
820 sensitivity is a major determinant of depolarization-induced retrograde sup-
821 pression at hippocampal synapses. *Journal of Neuroscience*, 22(10):3864–
822 3872, 2002.

- [58] Frauke Steindel, Raissa Lerner, Martin Häring, Sabine Ruehle, Giovanni Marsicano, Beat Lutz, and Krisztina Monory. Neuron-type specific cannabinoid-mediated g protein signalling in mouse hippocampus. *Journal of neurochemistry*, 124(6):795–807, 2013.
- [59] Sabine Ruehle, A Aparisi Rey, Floortje Remmers, and Beat Lutz. The endocannabinoid system in anxiety, fear memory and habituation. *Journal of Psychopharmacology*, 26(1):23–39, 2012.
- [60] Robert E Hampson and Sam A Deadwyler. Role of cannabinoid receptors in memory storage. *Neurobiology of disease*, 5(6):474–482, 1998.
- [61] Miles A Whittington and Roger D Traub. Interneuron diversity series: Inhibitory interneurons and network oscillations in vitro. *Trends in neurosciences*, 26(12):676–682, 2003.
- [62] Horacio G Rotstein, Dmitri D Pervouchine, Corey D Acker, Martin J Gillies, John A White, Eberhardt H Buhl, Miles A Whittington, and Nancy Kopell. Slow and fast inhibition and an h-current interact to create a theta rhythm in a model of ca1 interneuron network. *J Neurophysiol*, 94:1509–1518, 2005.
- [63] Can Tao, Guangwei Zhang, Ying Xiong, and Yi Zhou. Functional dissection of synaptic circuits: in vivo patch-clamp recording in neuroscience. *Frontiers in Neural Circuits*, 9:23, 2015.
- [64] Vasilis Z Marmarelis, Dae C Shin, Dong Song, Robert E Hampson, Sam A Deadwyler, and Theodore W Berger. On parsing the neural code in the prefrontal cortex of primates using principal dynamic modes. *Journal of Computational Neuroscience*, 36(3):321–337, 2014.
- [65] Dong Song, Rosa HM Chan, Vasilis Z Marmarelis, Robert E Hampson, Sam A Deadwyler, and Theodore W Berger. Nonlinear dynamic modeling of spike train transformations for hippocampal-cortical prostheses. *Biomedical Engineering, IEEE Transactions on*, 54(6):1053–1066, 2007.
- [66] George Paxinos and CH Watson. The rat brain in stereotaxic coordinates 2nd edn. *Academic Press, New York.*, 11(4):237–243, 1986.
- [67] Theodore W Berger, Dong Song, Rosa HM Chan, Vasilis Z Marmarelis, Jeff LaCoss, Jack Wills, Robert E Hampson, Sam A Deadwyler, and John J Granacki. A hippocampal cognitive prosthesis: multi-input, multi-output nonlinear modeling and vlsi implementation. *Neural Systems and Rehabilitation Engineering, IEEE Transactions on*, 20(2):198–211, 2012.
- [68] Sam A Deadwyler, Terence Bunn, and Robert E Hampson. Hippocampal ensemble activity during spatial delayed-nonmatch-to-sample performance in rats. *Journal of Neuroscience*, 16(1):354–372, 1996.
- [69] Robert E Hampson, Dong Song, Rosa HM Chan, Andrew J Sweatt, Mitchell R Riley, Anushka V Goonawardena, Vasilis Z Marmarelis, Greg A

- 862 Gerhardt, Theodore W Berger, and Sam A Deadwyler. Closing the loop
863 for memory prosthesis: Detecting the role of hippocampal neural ensembles
864 using nonlinear models. *Neural Systems and Rehabilitation Engineering*,
865 *IEEE Transactions on*, 20(4):510–525, 2012.
- 866 [70] Ude Lu, Dong Song, and Theodore W Berger. Nonlinear dynamic model-
867 ing of synaptically driven single hippocampal neuron intracellular activity.
868 *Biomedical Engineering, IEEE Transactions on*, 58(5):1303–1313, 2011.
- 869 [71] Dong Song, Rosa HM Chan, Vasilis Z Marmarelis, Robert E Hampson,
870 Sam A Deadwyler, and Theodore W Berger. Nonlinear modeling of neural
871 population dynamics for hippocampal prostheses. *Neural Networks*, 22(9):
872 1340–1351, 2009.
- 873 [72] Theodoros P Zanos, Spiros H Courellis, Theodore W Berger, Robert E
874 Hampson, Sam A Deadwyler, and Vasilis Z Marmarelis. Nonlinear model-
875 ing of causal interrelationships in neuronal ensembles. *Neural Systems and*
876 *Rehabilitation Engineering, IEEE Transactions on*, 16(4):336–352, 2008.
- 877 [73] James J. Higgins. *Intoruction to Modern Nonparametric Statistics*. 2003.
- 878 [74] James A Hanley and Barbara J McNeil. The meaning and use of the area
879 under a receiver operating characteristic (roc) curve. *Radiology*, 143(1):
880 29–36, 1982.
- 881 [75] Mark CW van Rossum. A novel spike distance. *Neural Computation*, 13
882 (4):751–763, 2001.
- 883 [76] Jonathan D Victor and Keith P Purpura. Metric-space analysis of spike
884 trains: theory, algorithms and application. *Network: computation in neural*
885 *systems*, 8(2):127–164, 1997.